

# Manipulation of atom number distributions in lattice-confined spinor gases

J. O. Austin,<sup>1</sup> Z. N. Shaw,<sup>1</sup> Z. Chen,<sup>1</sup> K. W. Mahmud,<sup>2,\*</sup> and Y. Liu<sup>1,†</sup>

<sup>1</sup>*Department of Physics, Oklahoma State University, Stillwater, Oklahoma 74078, USA*

<sup>2</sup>*Joint Quantum Institute, University of Maryland, College Park, Maryland 20742, USA*

(Dated: October 19, 2021)

We present an experimental study demonstrating the manipulation of atom number distributions of spinor gases after nonequilibrium quantum quenches across superfluid to Mott insulator phase transitions in cubic optical lattices. Our data indicate that atom distributions in individual Mott lobes can be tuned by properly designing quantum quench sequences, which suggest methods of maximizing the fraction of atoms in Mott lobes of even occupation numbers and have applications in attaining different quantum magnetic phases including massively entangled states. In addition, we find qualitative agreements between our experimental data and numerical simulations based on time-dependent Gutzwiller approximations in two-dimensional systems.

Possessing a spin degree of freedom, spinor Bose-Einstein condensates (BECs) can be combined with optical lattices and microwave dressing fields to offer a system with an exceptional level of control over many parameters, such as the number of interacting atoms, temperature, total spin of the system, the lattice potential, and dimensionality of the system [1–11]. Lattice-confined spinor BECs have thus been utilized to form highly programmable quantum simulators, which are capable of studying a vast array of topics at the forefront of physics research, especially those that are too computationally complex to study using classical computers [4, 7, 9]. One feature of lattice-confined spinor gases of particular interest is that atoms in Mott-insulator (MI) lobes of different occupation numbers can have distinct and potentially desirable properties, e.g., antiferromagnetic spinor gases can only form spin singlets in even Mott lobes [3, 10–14]. Many-body spin singlet states, which consist of massively entangled spin components, have been suggested as exemplary platforms for studying quantum memory and quantum metrology [7]. The number distribution of ultra-cold atoms in lattices has thus been a topic of great interest [8, 15–23]. Various experimental approaches have been realized to determine number distributions after atoms are loaded into deep lattices, such as direct imaging [16, 22], light scattering [15], and the detection of discrete energy signatures for each occupation number  $n$  [8, 19]. Despite these experimental successes, little work has been done to investigate how these measured distributions depend on parameters of quantum quenches, for example the quench speed. Further exploration of number distributions and their manipulation is warranted to potentially allow for the optimization of desirable qualities.

With spin-dependent interactions  $U_2$ , spinor gases exhibit both superfluidity and magnetism while presenting some other features which are absent in scalar bosons. One notable feature is coherent spin interconversions among multiple spin components resulting from the competition of  $U_2$  and the quadratic Zeeman energy  $q$  [2–5]. By analyzing these spin-mixing dynamics, the signa-

tures of discrete energy levels can be extracted from a Fourier analysis, and many interesting features of many-body ground states in spinor gases can be revealed [1, 8]. This approach has been developed in theory by Ref. [1] and experimentally verified for adiabatic ramps by our previous work [8]. In this paper, we extend this method to probe atom number distributions after nonadiabatic quantum quenches. Our data demonstrate that atom distributions can be manipulated by properly designing the quantum quench sequence, which may have important applications in attaining different many-body quantum phases. Our observations also suggest methods of maximizing the fraction of atoms in even Mott lobes which, among other things, may enable future works to optimize the production of massively entangled states in cold atoms. Another notable aspect of our experiment is the toolbox it provides for probing spinor atoms at the on-site level, which can be utilized to deduce the coefficients of the on-site wavefunction and calculate number fluctuations, spin-singlet order parameter, and various other entanglement observables in homogeneous systems [1, 7].

Similar to our previous work [4], we apply the Bose-Hubbard (BH) model and the Gutzwiller approximation to understand the static and dynamic properties of lattice-trapped spin-1 bosons and express the spin-1 BH

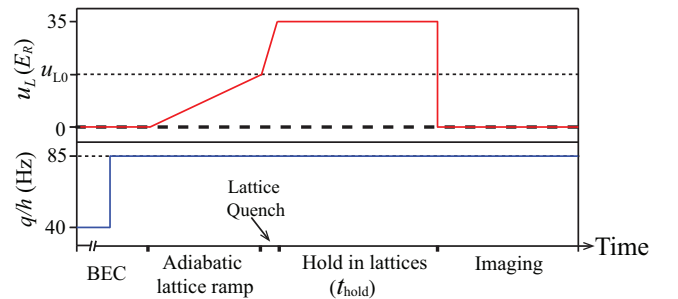


FIG. 1. Schematic of an experimental cycle of the Quench-L sequence (see text).  $u_{L0}$  is the intermediate lattice depth. Axes are not to scale.

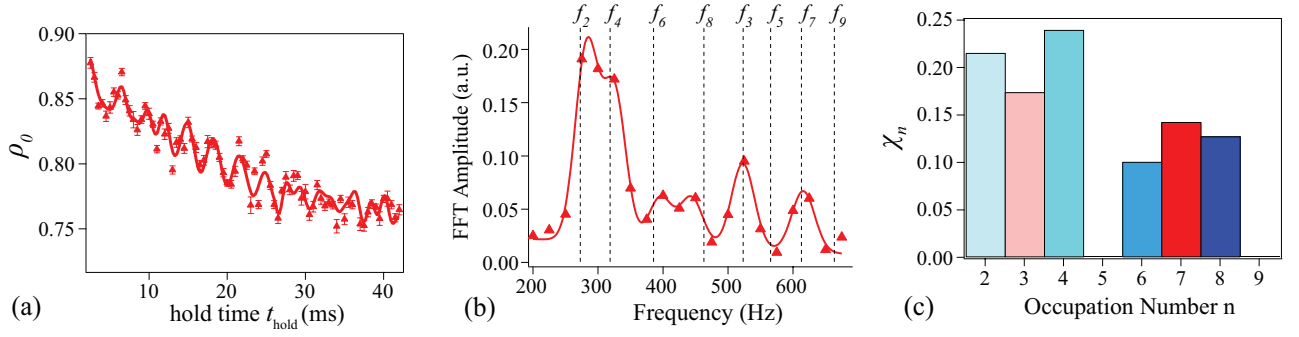


FIG. 2. (a) Observed dynamics of spin-0 atoms after a Quench- $L$  sequence at  $v_{\text{ramp}} = 14(1)E_R/\text{ms}$  and  $u_{L0} = 0E_R$  (see text and Fig. 1). Markers represent the average of approximately 15 repeated shots at the same conditions and error bars are one standard error. The solid line is a fit based on our empirical model to guide the eye [8]. (b) Markers show fast Fourier transformations (FFT) over the first 40 ms of  $t_{\text{hold}}$  on the data shown in Panel (a). Vertical lines mark the predicted energy signature  $f_n$  for each  $n$  (see text). The solid line represents Gaussian fits to each observed peak. (c) Number distributions  $\chi_n$  extracted from the FFT spectrum shown in Panel (b) (see text).

Hamiltonian as

$$\begin{aligned} \hat{H} = & -J \sum_{\langle i,j \rangle, m_F} (\hat{a}_{i,m_F}^\dagger \hat{a}_{j,m_F} + \hat{a}_{j,m_F}^\dagger \hat{a}_{i,m_F}) - \sum_i \mu_i \hat{n}_i \\ & + \frac{U_0}{2} \sum_i \hat{n}_i (\hat{n}_i - 1) + \frac{U_2}{2} \sum_i (\vec{F}_i^2 - 2\hat{n}_i) \\ & + \frac{1}{2} V_T \sum_i (i - \frac{L}{2})^2 \hat{n}_i + q \sum_i (\hat{n}_{i,1} + \hat{n}_{i,-1}). \end{aligned} \quad (1)$$

Here  $U_0$  is the spin-independent interaction,  $J$  is the tunnelling energy,  $\mu$  is the chemical potential,  $V_T$  is the external trapping potential,  $\vec{F}$  is the spin operator,  $\hat{n}_i = \sum_{m_F} \hat{n}_{i,m_F} = \sum_{m_F} \hat{a}_{i,m_F}^\dagger \hat{a}_{i,m_F}$  is the atom number operator at site- $i$ ,  $\hat{a}_{m_F}$  ( $\hat{a}_{m_F}^\dagger$ ) is the boson destruction (creation) operator for the spin- $m_F$  component,  $m_F$  can be 0 or  $\pm 1$  for  $F = 1$  atoms, and  $L$  is the number of lattice sites [1, 4]. In deep lattices where tunnellings among neighboring lattice sites are negligible, Eq. (1) can be further decoupled into the single site Hamiltonian [1, 8],

$$\hat{H} = \frac{U_0}{2} \hat{n}(\hat{n} - 1) + \frac{U_2}{2} (\vec{F}^2 - 2\hat{n}) + q(\hat{n}_1 + \hat{n}_{-1}) - \mu \hat{n}, \quad (2)$$

where  $\hat{n} = \sum_{m_F} \hat{n}_{m_F}$  is the atom number operator for each lattice site.

In the Gutzwiller approximation, the many-body wave function of the full lattice can be written as a product of single site states, which for a homogeneous system is  $|\phi\rangle = \sum_{n_1, n_0, n_{-1}} C_{n_1, n_0, n_{-1}} |n_1, n_0, n_{-1}\rangle$  in the Fock state basis  $|n_1, n_0, n_{-1}\rangle$ . Fock state coefficients  $P(n_1, n_0, n_{-1}) = |C_{n_1, n_0, n_{-1}}|^2$  define the Fock state number distributions. The Fock state coefficient for the spin-0 component is then denoted as  $\chi_n = \sum_{n_1, n_{-1}} |C_{n_1, n_0, n_{-1}}|^2$ , which can be obtained by performing Fourier analysis of the spin-mixing dynamics [1, 8]. A related quantity is the number density in each lattice site which is defined as  $N(n_0) = \sum_{n_1, n_{-1}} n_0 |C_{n_1, n_0, n_{-1}}|^2$ .

The Fock state coefficients and number densities for other spin components can be found by the same method.

For a homogeneous system,  $\chi_n$  reveals the on-site atom number statistics which displays a Poissonian behavior in a superfluid (SF) state and gets number squeezed in the MI regime, while  $N(n_0)$  gives the expectation value of the atom number or the average density of the atoms [23]. In our experimental systems, however, atoms in cubic lattices are externally confined in a harmonic trapping potential. This results in an inhomogeneous density profile with different atom number statistics at individual lattice sites. In the MI state, this leads to a wedding cake structure in the density profile with constant integer density Mott plateaus. For such an inhomogeneous system, each lattice site therefore has different on-site number statistics. The many-body wavefunction at site- $i$  can be expressed as  $|\phi_i\rangle = \sum_{n_{i,1}, n_{i,0}, n_{i,-1}} C_{n_{i,1}, n_{i,0}, n_{i,-1}} |n_{i,1}, n_{i,0}, n_{i,-1}\rangle$ . The atom number distributions and number density distributions in our system become site-dependent, e.g.,  $\chi_{n_i}$  and  $N(n_{i,0})$  represent the distributions of spin-0 atoms in the  $i$ -th lattice site. In our experiments, we collect data after releasing atoms from all trapping potentials, each observed number distribution is thus summed over all lattice sites, i.e.,  $\chi_n = \sum_i \chi_{n_i}$ .

We start each experiment cycle with a spinor BEC of approximately  $1.2 \times 10^5$  sodium ( $^{23}\text{Na}$ ) atoms at its SF ground state, the longitudinal polar state with  $\rho_0 = 1$  and  $m = 0$ . Here  $\rho_{m_F}$  is the fractional population of the  $m_F$  state and  $m = \rho_{+1} - \rho_{-1}$  is the magnetization. The spinor gases studied in this paper exhibit antiferromagnetic characteristics because  $U_2 = 0.035U_0 > 0$  [4, 8]. We then load atoms into a cubic optical lattice with a lattice spacing of 0.532 microns and continuously quench the lattice depth  $u_L$  through the SF to MI phase transition points via Quench- $L$  sequences at different speeds. The lattice depth is in the unit of the recoil energy  $E_R$  [4, 5, 8].

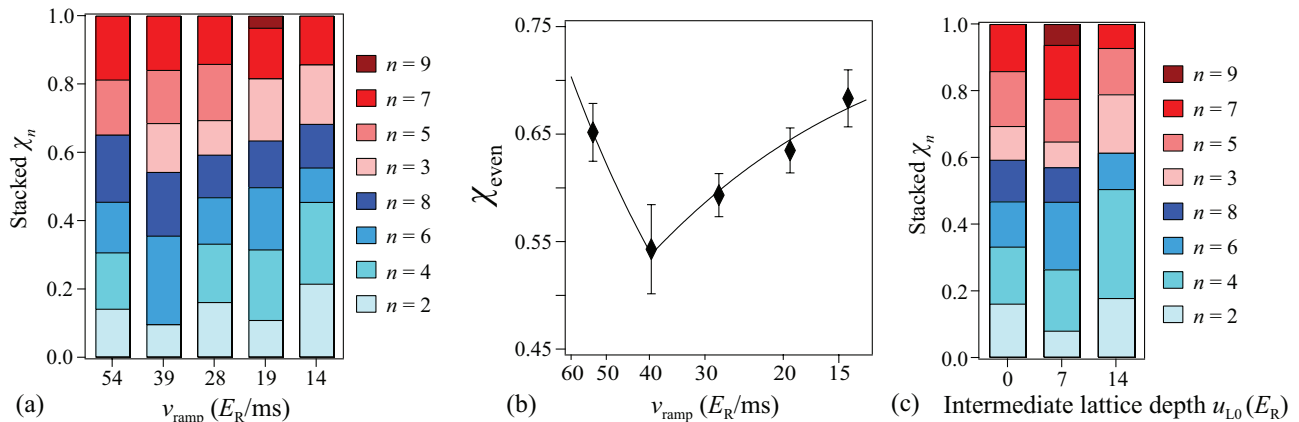


FIG. 3. (a) Observed number distributions  $\chi_n$  after Quench- $L$  sequences at various  $v_{\text{ramp}}$  and  $u_{L0} = 0E_R$ . Shades of blue (red) represent even (odd) occupation numbers  $n$  with the shades getting darker as  $n$  increases from 2 to 8 (from 3 to 9). The height of each shaded box represents  $\chi_n$  for a given  $n$ , while the combined height of the blue (red) boxes corresponds to the total number distribution in even (odd) Mott lobes. (b) Diamonds represent the experimentally found fraction of even Mott lobes  $\chi_{\text{even}}$  for each quench sequence shown in Panel (a). The solid line is a linear (an exponential) fit to the data when  $v_{\text{ramp}}$  is faster (slower) than 39(1) $E_R/\text{ms}$ . (c) Similar to Panel (a) but uses Quench- $L$  sequences with various  $u_{L0}$  while keeping  $v_{\text{ramp}}$  at 28(1) $E_R/\text{ms}$  during the lattice ramp from  $u_{L0}$  to 35 $E_R$  (see text).

Figure 1 shows the schematic of Quench- $L$  sequences, in which we first adiabatically raise  $u_L$  to an intermediate value  $u_{L0}$  at the ramp speed of  $1.4E_R/\text{ms}$  and then non-adiabatically quench  $u_L$  to a deep final lattice depth  $u_L^{\text{final}}$  at a faster speed  $v_{\text{ramp}}$  to initiate spin-mixing dynamics. Because  $u_L^{\text{final}}$  is much deeper than the SF-MI transition points, which are between  $16E_R$  and  $23E_R$  for our system of  $n_{\text{peak}} = 7$ , atoms are localized into individual lattice sites by the end of the quench sequence [3]. Here  $n_{\text{peak}}$  is the peak occupation number per lattice site in equilibrium MI states [4, 5, 8]. After the lattice quench, we hold the atoms at  $u_L^{\text{final}}$  for a holding time  $t_{\text{hold}}$  before abruptly releasing them, and then detect different spin components via a two-stage microwave imaging process [4, 7].

While  $q/h \lesssim 100$  Hz, spin dynamics similar to those presented in Fig. 2(a) are observed, where  $q$  is the quadratic Zeeman energy and  $h$  is Planck's constant. Consisting of multiple Rabi-type oscillations of frequencies  $f_n$ , these dynamics offer an ideal platform to probe the atom number distributions of spinor gases [1, 8]. Here  $f_n = E_n/h$ , while  $E_n$  is the energy gap between the first excited state and the ground state for a fixed  $n$  [1, 8]. When  $q$  and  $u_L^{\text{final}}$  are carefully chosen to be large enough that the frequencies of spin-mixing oscillations at individual  $n$  are well separated but  $q$  is small enough that the system still displays spin oscillations after quantum quenches, the resulting spin dynamics allow us to extract the number distributions of our system. In this paper, all data are collected at  $u_L^{\text{final}} = 35E_R$  and  $q/h = 85$  Hz which offers a good balance between these conditions. By conducting a fast Fourier transformation (FFT) over the first 40ms of each observed spin dynamics, we can

precisely determine the spectral weight of each oscillation and thus extract the atom number distributions after quenches at various  $v_{\text{ramp}}$ . We choose 40 ms for each FFT as it is sufficiently long to clearly resolve each peak while remaining short enough to avoid the number distribution changing significantly with  $t_{\text{hold}}$  during the data taking. The observed FFT spectra, similar to the one shown in Fig. 2(b), are then fit with an eight-Gaussian fitting. By integrating over each peak and dividing by the theoretical spin oscillation amplitude at each  $n$ , we can obtain the spectral contributions of individual  $n$  [8]. As shown in Fig. 2(c), when these values are normalized this process gives us the atom number distributions  $\chi_n$  in deep lattices for each integer  $n$ . Because no spin oscillations occur when  $n = 1$ , all  $\chi_n$  shown in this paper reflect the normalized number distributions after the  $n = 1$  Mott lobe is excluded.

The observed atom number distributions after Quench- $L$  sequences at various  $v_{\text{ramp}}$  are displayed in Fig. 3(a). Because the realizations and manipulations of some important quantum states (e.g. spin singlets) of ultracold atoms depend on the increased presence of even Mott lobes [3, 10–14], one parameter of particular significance that we wish to probe is  $\chi_{\text{even}}$ , the fraction of atoms in even Mott lobes. Figure 3(b) shows the observed  $\chi_{\text{even}}$  as a function of the lattice quench speed. As seen in Fig. 3(b), the distributions found at the fastest tested speed of  $v_{\text{ramp}} = 54(1)E_R/\text{ms}$  have a relatively high  $\chi_{\text{even}}$ , and there is a clear dip in  $\chi_{\text{even}}$  as the quench speed is lowered from  $54(1)E_R/\text{ms}$  to  $39(1)E_R/\text{ms}$ , which then increases exponentially with  $v_{\text{ramp}}$  back to a relatively high  $\chi_{\text{even}}$ . One notable result is that most observed  $\chi_{\text{even}}$  shown in Fig. 3(b) are larger than the predicted

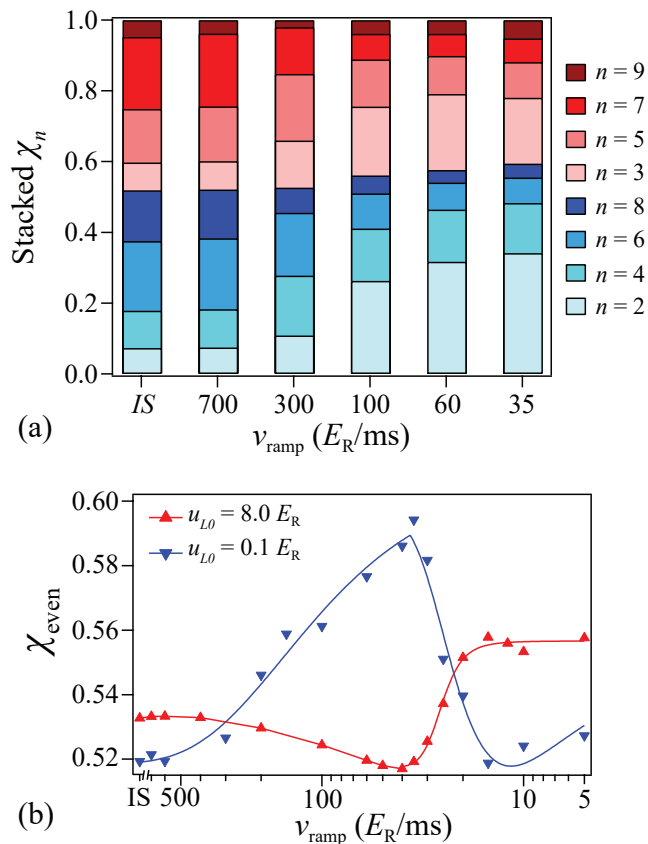


FIG. 4. (a) Predicted number distributions  $\chi_n$  derived from our numerical simulations for 2D lattice-confined sodium spinor gases after Quench- $L$  sequences with  $u_{L0} = 0.1E_R$  at various quench speeds  $v_{\text{ramp}}$  and for  $IS$ , the initial superfluid ground state. Shades of blue (red) represent even (odd)  $n$  with the shades getting darker as  $n$  increases from 2 to 8 (3 to 9). The height of each shaded box represents the predicted  $\chi_n$  for a given  $n$ , while the combined height of the blue (red) boxes represents the total number distributions in even (odd) Mott lobes. (b) Markers represent fractions of even Mott lobes extracted from simulated lattice quenches similar to those shown in Panel (a) but at various  $v_{\text{ramp}}$  and two  $u_{L0}$ . Solid lines are fitting curves to guide the eye.

$\chi_{\text{even}}$  of 0.55 for equilibrium MI states at  $n_{\text{peak}} = 7$ . We find no discernible FFT spectra can be obtained after Quench- $L$  sequences at slow speeds of  $v_{\text{ramp}} < 10E_R/\text{ms}$  because the amplitude of spin-mixing oscillations after the quenches appears to rapidly diminish as  $v_{\text{ramp}}$  decreases. As elaborated in our previous work [8], to study number distributions after adiabatic ramps, we thus have to use a Quench- $Q$  sequence, in which atoms first adiabatically cross the SF-MI phase transitions in a high magnetic field of  $q \gg U_2$  to ensure the atoms remain in their ground states and then spin dynamics are initiated by quenching the magnetic field to a desired final  $q$ .

We also examine the effects of varying the intermediate lattice depth  $u_{L0}$  at the start of the quench in Quench- $L$  sequences in Fig. 3(c). In these experiments, the lat-

tice ramp speed  $v_{\text{ramp}}$  is kept at  $28(1)E_R/\text{ms}$  during the quenches from various  $u_{L0}$  to the final lattice depth of  $35E_R$ . Our data in Fig. 3(c) indicate that the observed  $\chi_{\text{even}}$  only weakly depends on  $u_{L0}$  at this  $v_{\text{ramp}}$ . As  $u_{L0}$  increases and approaches SF-MI transition points, the maximum  $n$  extracted from the experimental FFT spectra appear to decrease and get close to the predicted  $n_{\text{peak}}$  for equilibrium MI states, which confirms lattice ramps become more adiabatic at larger  $u_{L0}$ .

Our experiments are performed in 3D inhomogeneous lattice-confined spin-1 spinor gases. An exact many-body simulation of such systems has not yet been reported in the literature either for equilibrium states or nonequilibrium dynamics [4]. This numerical problem is prohibitively difficult due to high Hilbert space dimensions of on-site spin-1 atoms and the inhomogeneous nature of the systems, and hence feasible theoretical simulations are limited to one and two dimensions (2D). Figure 4(a) shows typical simulation results of atom number distributions performed in systems similar to our experimental system but in 2D after Quench- $L$  sequences at various quench speeds and also for the initial SF ground state which corresponds to an infinitely fast ramp in Quench- $L$  sequences. Each predicted distribution shown in Fig. 4 is averaged over all lattice sites and only includes the experimentally observable Mott lobes of  $n \geq 2$ .

We find qualitative agreements between our 2D theoretical simulations and 3D experimental results, despite quantitative disparities which are expected due to the difference in dimensionality. For example, similar to our experimental data shown in Fig. 3(a), the simulated atom number distributions in Fig. 4(a) indicate a dependence on the lattice quench speed  $v_{\text{ramp}}$ . The predicted even fractions after simulated quenches at various  $v_{\text{ramp}}$  (see Fig. 4(b)) also display some similarities to our experimental observations illustrated in Fig. 3(b), e.g.,  $\chi_{\text{even}}$  exponentially increases from a value around the predicted  $\chi_{\text{even}}$  for the initial SF ground state as  $v_{\text{ramp}}$  is lowered, and  $\chi_{\text{even}}$  reaches its maximum at a nonadiabatic quench speed. Our theoretical results indicate that  $\chi_{\text{even}}$  should decrease to the value for equilibrium MI states as  $v_{\text{ramp}}$  continues to decrease but because we are unable to observe spin oscillations at very small  $v_{\text{ramp}}$ , we have not been able to observe this experimentally. Differences between the two theory curves in Fig. 4(b) also imply that it is possible to optimize the even fraction  $\chi_{\text{even}}$  by properly designing the quantum quench sequence, e.g., larger maximum achievable  $\chi_{\text{even}}$  may be realized at smaller  $u_{L0}$ . These results suggest that atoms go through complex spatial dynamics while redistributing within the harmonic trap during the quantum quenches, and number distributions reach an equilibrium value when the quench speed is sufficiently slow to ensure the atoms initially located in the trap center have enough time to move towards the trap boundaries and equilibrate. Note that Gutzwiller approxima-

tion ignores all inter-site correlations and entanglement to compute the ground state properties and the dynamics. The spinor system near SF-MI transitions, however, is a highly correlated system where inter-site correlations may need to be considered for a more rigorous analysis. Other numerical methods may be better suited to study this phenomenon, but we are further limited by dimensionality, i.e., we can only conduct simulations in 1D or 2D systems rather than 3D systems. Density Matrix Renormalization Groups (DMRG) algorithms in particular might yield valuable insight but are only efficient in 1D systems [4]. An efficient high performance computation of 3D lattice-confined spinor systems is a planned future research avenue for improving the theory-experiment comparisons.

In conclusion, we have experimentally demonstrated the manipulation of atom number distributions of lattice-confined spinor gases after nonadiabatic quantum quenches. Our data have illustrated methods of maximizing the fraction of atoms in even Mott lobes, which have applications in attaining various quantum magnetic phases including massively entangled states. Qualitative agreements have also been found between our experimental data and numerical simulations using time-dependent Gutzwiller approximations in two-dimensional systems.

We thank the National Science Foundation and the Noble Foundation for financial support.

---

\* Present address: Quidient LLC, Columbia, MD 21046

† Electronic address: yingmei.liu@okstate.edu

- [1] K. W. Mahmud and E. Tiesinga, Dynamics of spin-1 bosons in an optical lattice: spin mixing, quantum-phase-revival spectroscopy, and effective three-body interactions, *Phys. Rev. A* **88**, 023602 (2013).
- [2] L. Zhao, J. Jiang, T. Tang, M. Webb, and Y. Liu, Dynamics in spinor condensates tuned by a microwave dressing field, *Phys. Rev. A* **89**, 023608 (2014).
- [3] J. Jiang, L. Zhao, S.-T. Wang, Z. Chen, T. Tang, L.-M. Duan, and Y. Liu, First-order superfluid-to-Mott-insulator phase transitions in spinor condensates, *Phys. Rev. A* **93**, 063607 (2016), and the references therein.
- [4] J. O. Austin, Z. Chen, Z. N. Shaw, K. W. Mahmud, and Y. Liu, Quantum critical dynamics in a spinor Hubbard model quantum simulator, *Communications Physics* **4**, 61 (2021), and the references therein.
- [5] L. Zhao, J. Jiang, T. Tang, M. Webb, and Y. Liu, Antiferromagnetic spinor condensates in a two-dimensional optical lattice, *Phys. Rev. Lett.* **114**, 225302 (2015).
- [6] N. T. Phuc, Y. Kawaguchi, and M. Ueda, Effects of thermal and quantum fluctuations on the phase diagram of a spin-1  $^{87}\text{Rb}$  Bose-Einstein condensate, *Phys. Rev. A* **84**, 043645 (2011).
- [7] L. Zhao, T. Tang, Z. Chen, and Y. Liu, Lattice-induced rapid formation of spin singlets in spin-1 spinor condensates, arXiv:1801.00773 (2018).
- [8] Z. Chen, T. Tang, J. Austin, Z. Shaw, L. Zhao, and Y. Liu, Quantum quench and nonequilibrium dynamics in lattice-confined spinor condensates, *Phys. Rev. Lett.* **123**, 113002 (2019).
- [9] I. Bloch, Ultracold quantum gases in optical lattices, *Nature Physics* **1**, 23-30 (2005).
- [10] A. Imambekov, M. Lukin, and E. Demler, Spin-exchange interactions of spin-one bosons in optical lattices: singlet, nematic, and dimerized phases, *Phys. Rev. A* **68**, 063602 (2003).
- [11] M. Lacki, S. Paganelli, V. Ahufinger, A. Sanpera, and J. Zakrzewski, Disordered spinor Bose-Hubbard model, *Phys. Rev. A* **83**, 013605 (2011).
- [12] E. Demler and F. Zhou, Spinor bosonic atoms in optical lattices: symmetry breaking and fractionalization, *Phys. Rev. Lett.* **88**, 163001 (2002).
- [13] M. Snoek and F. Zhou, Microscopic wave functions of spin-singlet and nematic Mott states of spin-one bosons in high-dimensional bipartite lattices, *Phys. Rev. B* **69**, 094410 (2004).
- [14] S. K. Yip, Dimer state of spin-1 bosons in an optical lattice, *Phys. Rev. Lett.* **90**, 250402 (2003).
- [15] R. Landig, L. Hruby, N. Dogra, M. Landini, R. Mottl, T. Donner, and T. Esslinger, Quantum phases from competing short-and long-range interactions in an optical lattice, *Nature* **532**, 476-479 (2016).
- [16] G. K. Campbell, J. Mun, M. Boyd, P. Medley, A. E. Leanhardt, L. G. Marcassa, D. E. Pritchard, and W. Ketterle, Imaging the Mott insulator shells by using atomic clock shifts, *Science* **313**, 649-652 (2006).
- [17] A. K. Tuchman, C. Orzel, A. Polkovnikov, and M. A. Kasevich, Nonequilibrium coherence dynamics of a soft boson lattice, *Phys. Rev. A* **74**, 051601(R) (2006).
- [18] T. Zhou, K. Yang, Z. Zhu, X. Yu, S. Yang, W. Xiong, X. Zhou, X. Chen, C. Li, J. Schmiedmayer, X. Yue, and Y. Zhai, Observation of atom-number fluctuations in optical lattices via quantum collapse and revival dynamics, *Phys. Rev. A* **99**, 013602 (2019).
- [19] S. Will, T. Best, U. Schneider, L. Hackermüller, D.-S. Lühmann, and I. Bloch, Time-resolved observation of coherent multi-body interactions in quantum phase revivals, *Nature* **465**, 197-201 (2010).
- [20] A. Agarwala, M. Nath, J. Lugani, K. Thyagarajan, and S. Ghosh, Fock-space exploration by angle-resolved transmission through a quantum diffraction grating of cold atoms in an optical lattice, *Phys. Rev. A* **85**, 063606 (2012).
- [21] E. Tiesinga and P. R. Johnson, Collapse and revival dynamics of number-squeezed superfluids of ultracold atoms in optical lattices, *Phys. Rev. A* **83**, 063609 (2011).
- [22] W. S. Bakr, A. Peng, M. E. Tai, R. Ma, J. Simon, J. I. Gillen, S. Foelling, L. Pollet and M. Greiner, Probing the superfluid-to-Mott insulator transition at the single-atom level, *Science* **329**, 547-550 (2010).
- [23] B. Capogrosso-Sansone, E. Kozik, N. Prokofev, and B. Svistunov, On-site number statistics of ultracold lattice bosons, *Phys. Rev. A* **75**, 013619 (2007).